INSTITUTE OF PLASMA PHYSICS
CZECHOSLOVAK ACADEMY OF SCIENCES

LHCD EXPERIMENTS ON TOKAMAK CASTOR

Žáček F., Badalec J., Jakubka K., Kryška L., Preinhaelter J.,
Stoeckel J., Valovič M.,
Institute of Plasma Physics, Prague, Czechoslovakia

Nanobashvili S.,
Institute of Physics, Tbilisi, USSR

Weixelbaum L., Wenzel U.,
Central Institute of electron Physics, Berlin ,GDR

Spineanu F., Vlad M.,
Institute of Physics and Technology of Radiation Devices, Bucharest, Romania

RESEARCH REPORT

IPPCZ – 304

October 1990

POD VODÁRENSKOU VĚŽÍ 4, 180 69 PRAGUE 8
CZECHOSLOVAKIA

LHCD EXPERIMENTS ON TOKAMAK CASTOR

Žáček F., Badalec J., Jakubka K., Kryška L.,

Preinhaelter J., Stoeckel J., Valovič M.,

Institute of Plasma Physics, Prague, Czechoslovakia

Nanobashvili S.,

Institute of Physics, Tbilisi, USSR

Weixelbaum L., Wenzel U.,

Central Institute of electron Physics, Berlin, GDR

Spineanu F., Vlad M.,

Institute of Physics and Technology of Radiation

Devices, Bucharest, Romania

IPPCZ-304 October 1990

ABSTRACT

A short survey of experimental activity on small Prague tokamak CASTOR is given. This activity concerns first of all the LH current drive using multijunction waveguide grills as launching antennae. During two last years the effort was concentrated on the investigation of the electrostatic and magnetic fluctuations under conditions of comgined inductive/ /LHCD regimes and linking of those fluctuations level with the anomalous particles transport in tokamak CASTOR. These results are discussed in more detail.

INTRODUCTION

Tokamak CASTOR |1| is a small tokamak with following parameters: R=0.4m, a=0.085m, $I_p \leq 30$kA, $B_T \leq 2$T, $\tau \leq 50$ms. It has six diagnostic sections, every with three ports (from top, down and horizontal outer side). Two sections with great horizontal ports 80x200 mm make possible to use waveguide grills as LH wave launcher. A top view of the tokamak CASTOR is given in Fig. 1 together with the most important diagnostic tools.

The main object of experimental study on the CASTOR is concentrated on the RF wave-plasma interaction in lower hybrid region (f=1.25GHz, $P_{RF} \leq 40$ kW). The description

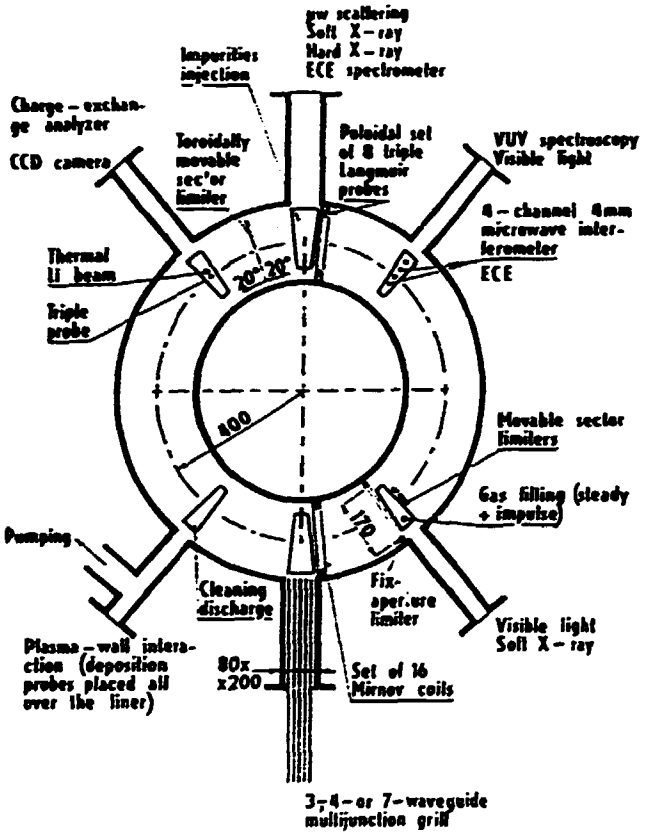

of the RF experiments, main diagnostics used and some results concerning RF current drive are given in Section 2. Section 3 brings methodics and the main results obtained at the measurements of plasma electrostatic and magnetic fluctuations, especially their suppression during the combined OH/LHCD regimes in CASTOR.

Fig. 1. Toroidal geometry of the tokamak CASTOR with schematical set-up of RF experiments and the most important diagnostic tools.

Finally, in Section 4 the conclusions are given.

2. STUDY OF LOWER HYBRID CURRENT DRIVE

For the LH experiments on CASTOR tokamak simple multijunction waveguide grills [2, 3] with seven (cross-section 5x160mm), four (10x160mm) and three (14x160mm) waveguides were developed and used. The cross-section view of the tokamak plasma and 4-waveguide multijunction grill is shown in Fig. 2. The orientation of all grills is such that the radiated power propagates predominantly in the direction of the electron drift velocity due to the inductive voltage.

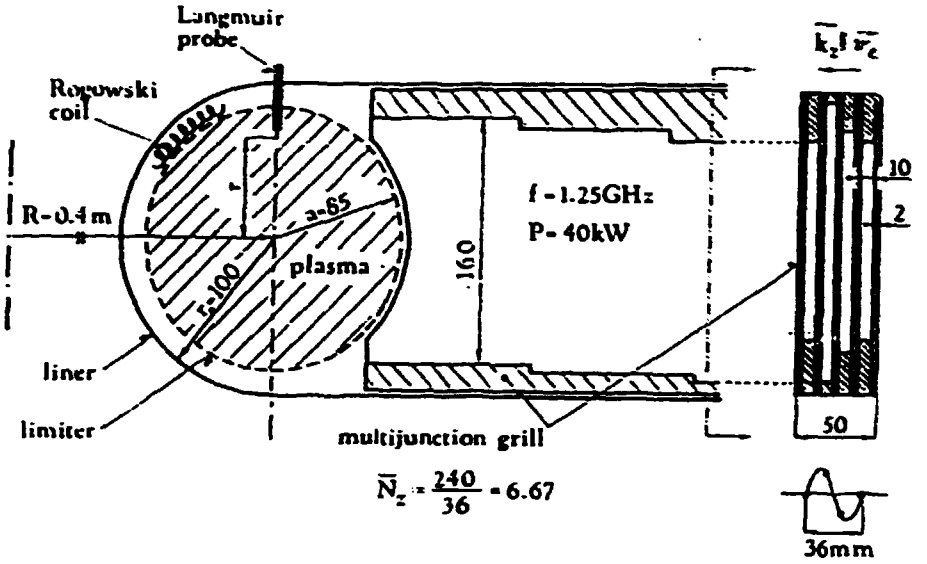

Fig. 2. Cross-section view of the tokamak plasma and 4-waveguide multijunction grill.

The four- and seven-grills have the phase shift between adjacent waveguides 120^0, the 3-grill has shift 90^0. Spectral power densities of the waves irradiated by these grills, enumerated in |4| for plasma density in the grill mouth $n_e=3\times10^{18}m^{-3}$ with a radial gradient $\nabla n_e=10^{20}m^{-4}$, are given in Fig. 3. It is possible to see that the maxima of these irradiated spectra extend from shortwavelength ($N_z>10$) to the longwavelength ($N_z<2$) region. The power transmitted through parasitic branches of the spectra ($N_z<0$) is in all three cases lower as 20 % and total power reflection coefficient does not exceed 30 %.

We must note, however, that such picture is true only for plasma parameters given above. Namely, if the plasma density in the grill mouth is lowered, the situation is changing drastically. As we have shown in |4|, the value of this density has much stronger effect on the multijunction grill efficiency than it is in the case of conventional grill. While the conventional grill tends to conserve the form of irradiated power spectrum regardless of the

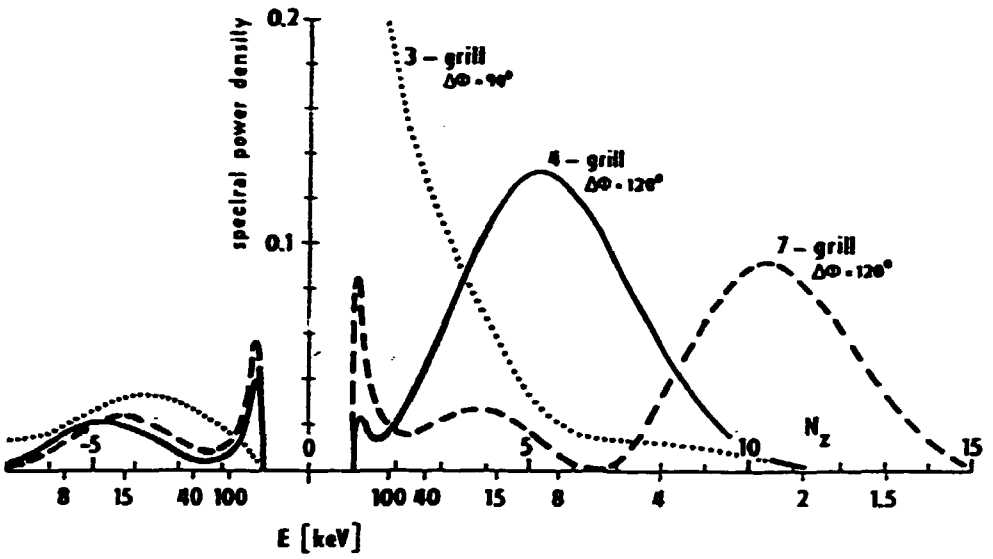

Fig. 3. Spectral power densities of the 3-, 4- and 7-waveguide multijunction grills.

decreasing density (the only response is an increasing reflection coefficient), the spectrum of multijunction grill varies strongly in this case, without significant increase of total reflected power. Due to this fact of selfadaption, the multijunction grill radiates RF power effectively even at low plasma densities, but in the spectrum the waves with $N_z \gtrsim 1$ are preferred (actually vacuum wave irradiated by open waveguide). Moreover, some of subsidiary waveguides of multijunction grill may be severely overloaded in this case. Note, that peripheral density can be easily influenced by changing of the plasma position or by non-linear effects due to the RF wave itself [5]. This drawback of multijunction grill is compensated, however, by its extreme simplicity making possible to assemble high power antenna systems with many hundreds of waveguides needed for the LHW application on the great tokamaks.

Due to the electrotechnical parameters of tokamak circuits the occurrence of the RF current in combined

OH/LHCD regimes is manifested predominantly by drop of voltage U_L on the plasma loop |6| and the increase of total plasma current is not significant. Both these fundamental quantities are measured by standard electrotechnical methods. Another important diagnostic tools see Fig. 1. Plasma density is measured in one cross-section by 4mm interferometer, SXR by a proportional SiLi detector (HPA) or SBD, HXR using NaI scintillators. A microwave diode for the band of 8mm was used as the ECE level registration. Using a He-cooled InSb detector with a fast-scanning Fourier spectrometer it was possible to estimate the energy and number of electrons accelerated by wave |7|. Movable Langmuir probes enabled us to carry out the density and temperature profiles measurements. It was possible to use these probes in some special regimes of experiment with purely LHW sustained plasma (see Sec. 2.1 below) all over the $r \gtrsim a/2$ without substantial plasma disturbance and probes damage. The density profiles, approximately in the same range of radius, but for or OH/LHCD regimes was measured using the Li thermal beam |8|. The local heat flux at the plasma edge, integrated over the whole tokamak pulse, was measured by a movable thermocouple probe.

Using the multijunction grill antennae described above three types of experiments were carried out. We mention them below more in detail.

2.1 Combined OH/LHCD Regimes

These experiments represent the main physical investigation on the CASTOR tokamak. A short RF pulse ($\tau < 5ms \ll \tau_{OH}$) is applied to the ohmically heated plasma during the quasi-stationary phase of tokamak discharge |9|. Typical temporal evolution of the plasma current, loop voltage, plasma density, H_β -line intensity, HXR intensity, ECE, CV and CIII carbon optical line intensities and excentricity factor

$\Lambda = \beta_p + l_i/2$ without (full lines) and with (dotted lines) RF power P_{RF}=40kW launched by the 4-waveguide grill are depicted in Fig. 4. The value of the RF driven current $I_{RF} = I_p \cdot (\Delta U_L / U_L)$ evaluated from the loop voltage drop U_L in discharge with I_p=10kA, is given for the same P_{RF}=40kW in Fig. 5 in dependence on the average plasma density $\bar{n}_e$ together with the rate of current increase. Fig. 6 shows an dependence of I_{RF} on the injected power for $\bar{n}_e$ = $6 \times 10^{18} m^{-3}$ and I_p=10kA.

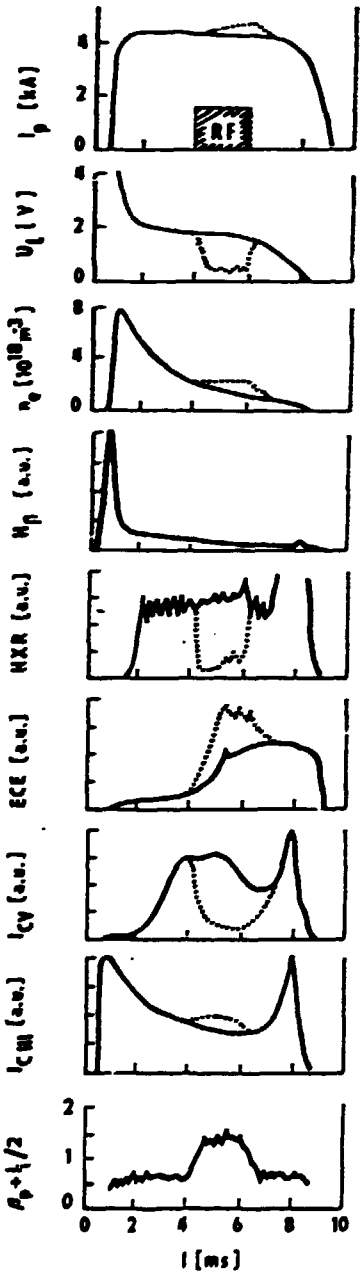

Fig. 4. Temporal evolution of the plasma parameters without (full lines) and with (dotted lines) application of RF power P_{RF}=40kW using the 4-waveguide grill.

The main results of these experiments may be summarized as follows:

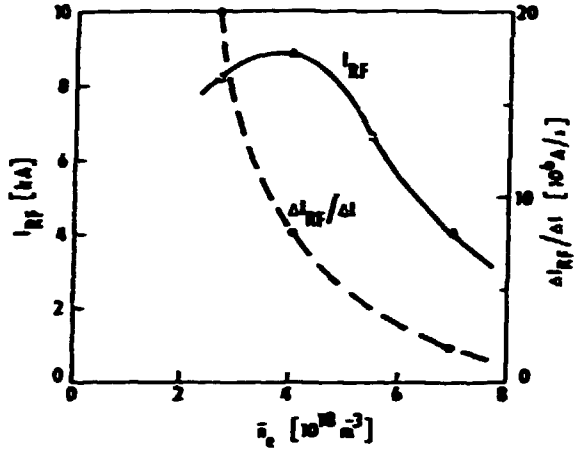

Fig. 5. Dependence of the RF driven current I_{RF} and current increase rate $\Delta I_{RF}/\Delta t$ for P_{RF} = = 40 kW on the plasma average density.

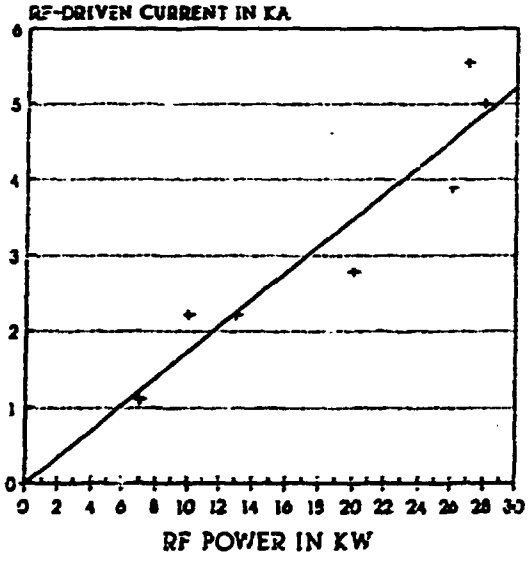

Fig. 6. Dependence of the RF current on the injected power for $\bar{n}_e = 6 \times 10^{18} m^{-3}$ and I_p = 10kA.

(1) taking into account both the power reflections and the launcher directivity, the RF-driven current is generated with a maximum efficiency 0.5-1A/W; the maximum value of RF current $I_{RF} \simeq 10$kA corresponds well to the theoretical estimation |10| for our parameters:

$$I_{RF} = 0.1 \times \delta \times T_e[keV] \times P_{RF}[kW] / (R[m] \times n_e[10^{13} cm^{-3}])$$

(δ =2-10 in dependence on the antenna power spectrum);

(2) occurrence of this current is manifested predominantly by drops in the loop voltage, an increase of ECE, suppression of HXR and by increase of $\Lambda = \beta_p + \ell_i/2$ |11|;

(3) the maximum measured initial rise of the RF current achieved value of $\Delta I_{RF}/\Delta t \simeq 2 \times 10^{7}$ A/s and initial rate of rise Λ the value $\dot{\Lambda} = 1.6 \times 10^{-3} s^{-1}$; it corresponds to about 20 % of the RF power absorption during this phase;
(4) during OH/LHCD regimes is the amplitude of non-thermal ECE proportional to the RF current; fast electrons with energy about 60keV and total number $\simeq 7 \times 10^{13}$ were deduced from the ECE spectra |7|; a significant role of these electrons, e.g. in the local heat Q deposited on the thermocouple probe, see in Fig. 7, where radial profiles of Q are given for pure OH and for OH/LHCD discharge with P_{RF}=15 and 30kW;

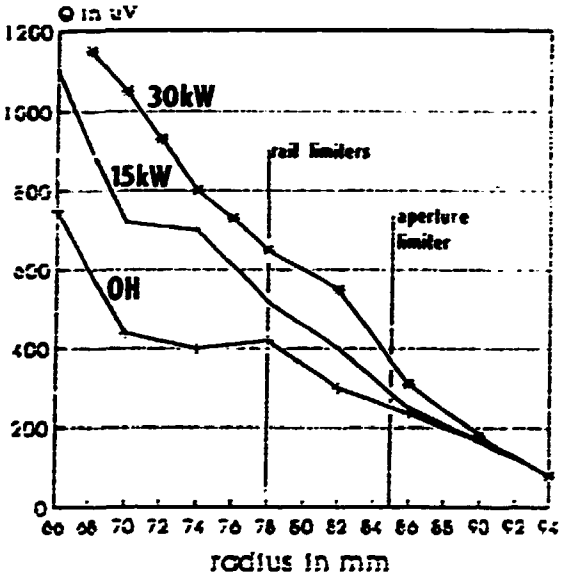

Fig. 7. Comparison od radial dependences of heat Q deposited on the thermocouple probe in OH and combined OH/LHCD discharges; τ_{OH}=40ms, RF pulse with τ_{RF}=5ms was applied in the stationary OH phase (between 15-20ms).

(5) with exception of the very low densities the current efficiency is inversely proportional to the plasma average density; the density limit for the current drive under our experimental conditions seems to be $\simeq 10^{19} m^{-3}$;
(6) following optical measurements, a certain plasma cooling takes place in the RF current-drive regime due to the OH power decrease;
(7) simultaneous analysis of H_β-line intensity and electron density time evolution suggests an substantial improvement of particle confinement time in combined OH/LHCD regimes;

this conclusion is supported by measurements of electron density gradient in OH and OH/LHCD regimes using a thermal Li beam, see Fig. 8, where some steepening of density profile with RF is documented;

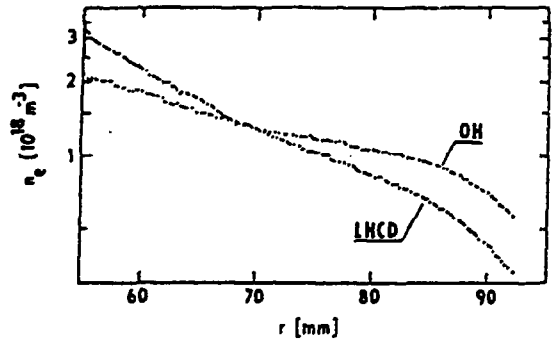

Fig. 8. Comparison of edge electron density profiles in the OH and combined OH/LHCD discharges.

(8) dependence of the RF current on the injected power seems to have a linear character for our accessible power.

2.2 LHCD Operation with OH Start

In these experiments the tokamak plasma was built by a standard OH scenario as described in the previous paragraph. However, in the moment when full plasma ionization was reached the primary coil of transformer was short-circuited and the plasma decay began. At some moment after the short-circuiting a long RF pulse was applied, see Fig. 9. After some transition period only a RF-driven current-sustained plasma during the whole RF period existed under assumption that the starting density was still sufficiently high ($\bar{n}_e \simeq 2 \times 10^{18} m^{-3}$). In opposite case the plasma decay continued due to the bad power coupling without any RF effect [9]. The parameters of the RF current-sustained plasma differed substantially from those in the OH inductive regime. Cooling of the main plasma body and flattening of its density distribution were the most important changes. The latter is demonstrated in Fig. 10, where the time dependence and radial distribution of the ion saturated current measu-

red by a movable Langmuir probe is given for three characteristic time: t_1-OH plasma, t_2-decaying plasma just before the onset the RF current drive, t_3-stationary RF current-sustained plasma.

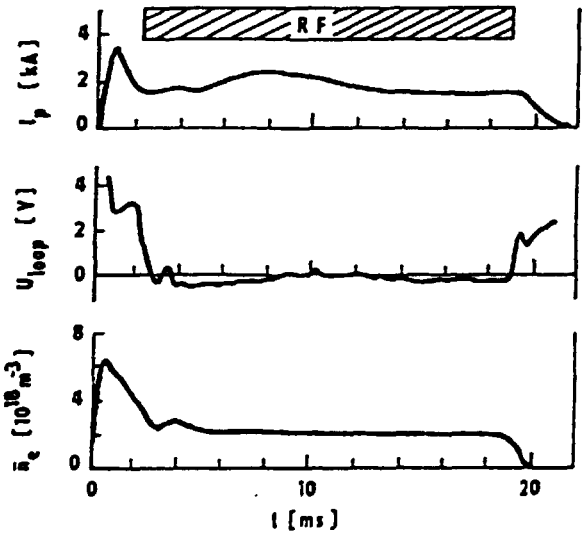

Fig. 9. Temporal evolution of plasma current, loop voltage and average electron density of the RF-driven current-sustained plasma.

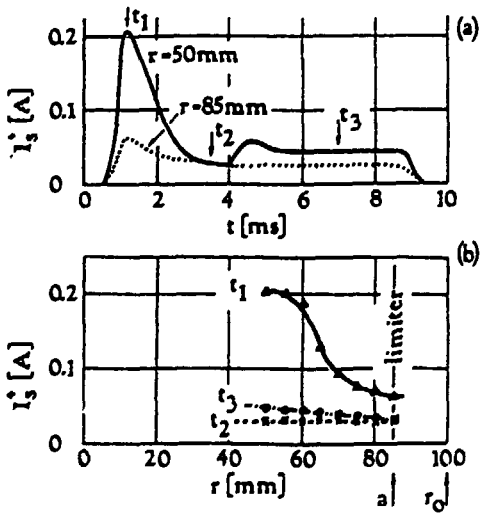

Fig. 10. a) Time dependence of the ion saturated current on the Langmuir probe located at radial position 50mm and 85mm.
b) Radial distribution of the ion saturated current in the OH and in the stationary RF current-sustained plasma.

Results of these experiments may be summarized as follows:
(1) by short-circuiting of the transformer primary coil, a quasistationary RF-driven current-sustained, low temperature plasma with a zero or slightly negative voltage was produced for the whole RF injection period ($\lesssim$ 25ms);
(2) line-average density of this plasma tends to be constant in time and equals $\bar{n}_e \simeq 2\times10^{18} m^{-3}$ for RF power R_{RF}=40kW;
(3) according to the probe measurements the radial distribution of density in such purely LHCD plasma is very flat; it is quite reasonable to suppose that profile of current density is very flat also - a certain current distribution flattening in the case of LHCD is predicted by theory |12| and moreover it has been already observed directly, e.g. in tokamak ASDEX |13| (note, however, that this must not be on the contrary case of density profile, see e.g. Fig. 8);
(4) RF current drive regime is characterized by an enhanced level of integral ECE, what indicates the existence of a group of current carrying electrons produced by LH wave; this assumption was fully confirmed by analysis of ECE spectra obtained with fast-scanning Fourier spectrometer and InSb detectors working in the spectral range 30-300GHz |7|.

2.3 Purely Non-Inductive RF operation

The multijunction grill has the fix phase shift between subsidiary waveguides given by construction. This fact makes impossible to use such grill for the simple RF gas breakdown and following plasma generation in LH frequency region. As the tokamak CASTOR is not equipped by ECE generator we tried to use another very simple scenario for the purely non-inductive RF operation. Namely, the RF power was applied simultaneously with the startup of the toroidal magnetic field B_T |14|. When the B_T increased from zero, the zone of ECR ($B_T \simeq 0.05$T for f=1.25GHz) arose at the inner side of

the vacuum chamber at time $t \simeq 0.5$ms and ECR plasma with density $\bar{n}_e \simeq 2 \times 10^{18} m^{-3}$ and T_e=10-40eV was created. Due to the mechanism of waves transformation |15| this plasma persisted during the whole RF pulse, in spite of the fact that no ECR zone existed more in the plasma. Moreover, the toroidal current generated by RF wave was also observed. However, the current drive efficiency was very low (I_p a few hundreds of A only) and due to poor confinement (no feed-back stabilization was used in this case) the plasma density and current continuously decreased during the RF pulse. Nevertheless, plasma could be sustained for the period up to 50ms (halfperiode of CASTOR toroidal magnetic field was only 60ms).

3. ELECTROSTATIC AND MAGNETIC FLUCTUATIONS DURING THE COMBINED INDUCTIVE/LOWER HYBRID CURRENT DRIVE ON CASTOR TOKAMAK

In present-day tokamaks, the experimentally determined electron confinement time τ_E is roughly two orders of magnitude lower than the neoclassical predictions. Generally, this anomalous transport has been atributed to microscopic plasma turbulence. A very large amount of theoretical and experimental work was devoted in the last 15 years to understanding the cause of the turbulence and its effect on the energy and particle transport. However, besides the important progresses obtained in this field, there are a lot of fundamental open questions which have to be answered in the future.

A review of turbulence and anomalous transport /16/ identified both magnetic and electrostatic turbulences as candidates for inducing anomalous transport, but also concluded that their relative importance is unknown up to now. However, the close correlation between the edge particle transport and electrostatic turbulence in OH regimes has

been observed on number of tokamaks /17-23/ as well as the correlation between anomalous energy losses and magnetic fluctuation level /24, 25/ (especially in additionally NBI and ICR heated plasmas). Generally may be said that a systematic increase of magnetic activity with decreasing energy confinement time τ_E is observed during the additional heating and thus a possible link between the energy confinement and magnetic fluctuation level is inferred.

A certain particle and energy confinement improvement during the combined OH-LHCD regimes was observed under some experimental conditions (application of moderate RF power $P_{RF} \lesssim P_{OH}$) in some tokamaks /28-33/. This effect was observed also on the CASTOR tokamak. It was the reason for experimental investigation of electrostatic /34-36/ and magnetic /37/ fluctuations in the combined OH/LHCD regimes on this tokamak in a few last years. The geometry of experiment and diagnostics enabling us to make these measurements with poloidal resolution are given in Fig. 11.

3.1 Edge Electrostatic Turbulence and Cross Field Induced Particle Transport

It was concluded by analysis made in /38/ for OH plasma in tokamak CASTOR that two main driving sources for the observed anomalous particle transport are present:
1) most part of the plasma cross-section (including the center) is affected by the dissipative drift instability driven by the density gradient relaxation;
2) at the border of the plasma the presence of an equilibrium radial electric field (observed in experiments) imposses a different type of instability driven by the relaxation of the vorticity gradient.

This conclusion follows from a numerical estimations of various parameters related to growth rate and fluctuations level starting from the experimental data on turbulence. The

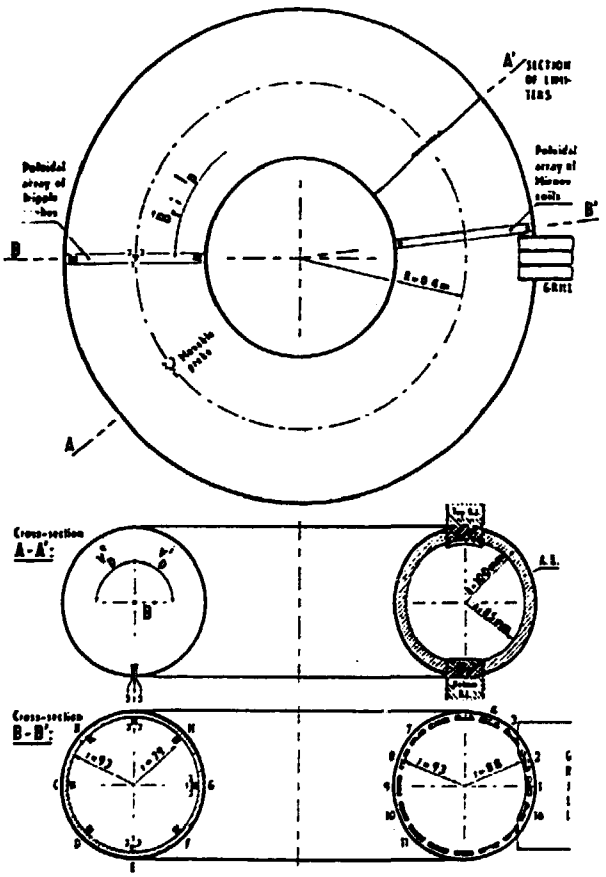

Fig. 11. The geometry of experiment and spacing of diagnostic tools for fluctuation measurements.

estimation of the relative level of the fluctuations excited by these microinstabilities in the CASTOR plasma gives in the center region value $\simeq 3\%$ and in the outer region value $\simeq 40\%$. This is in a very good agreement with experimental observations, see below Fig. 15. It was shown further from this fluctuation level and from the width of the observed frequency spectra, that above mentioned instabilities are deeply in the turbulent phase, in which the strong nonlinearity provides coupling in the wave number space, allowing thus the flow of energy.

Experimental set up.

The edge electrostatic turbulence on the tokamak CASTOR is investigated locally by a movable triple Langmuir probe

P_1, P_2, P_3 connected with a three-channel analog correlator /39/ allowing to monitor the root-mean-square (RMS) values of the electrostatic fluctuations (density n_e and poloidal electric field E_p) together with the time-average radial turbulent flux Γ. The arrangement of the triple probe in the tokamak vessel is schematically shown in Fig. 12. The tips of the probe are spaced in the form of a triangle with distance d=5mm (the probe with d=2-5mm were tested with similar results).

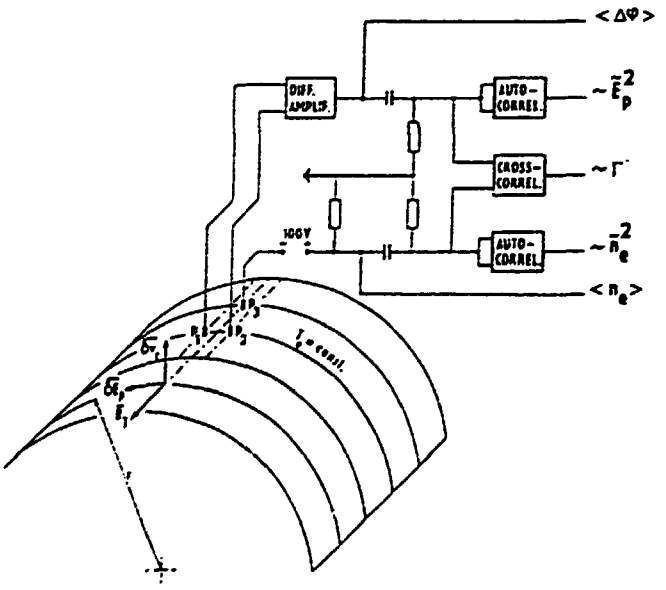

Fig. 12. Schematical arrangement of correlation measurements of the plasma fluctuations.

The two tips spaced poloidally are on the floating potential U_f and serve for the determination of space potential fluctuation $\delta\varphi = \delta U_f$, as for maxwellian hydrogen plasma $U_f \simeq \varphi - 3 \cdot T_e/e$ and the fluctuations of the electron temperature are assumed to be negligible at the plasma boundary, see /20/. The fluctuating part of the differential signal of these two floating probes ΔU_f is therefore proportional to the value of fluctuations of poloidal electric field δE_p. However, it should be noted that only E_p-fluctuations with poloidal wavenumber $k < 2\pi/d$ may be registered correctly.

The density fluctuations δn_e are deduced from the ion saturated durrent I_s on the third probe, biased at -150V with respect to the liner

$$\delta n_e = 2.\,\delta I_S/(A_P.c_S.e),$$

where A_P is the probe area, $c_S=\sqrt{T_e/m_i}$ is ion sound velocity, m_i is mass of ions.

The experimentally observed fluctuations of the poloidal electric field E_P lead to fluctuation δv_r of the particle velocity v_r and particle radial position /16/. For low-frequency fluctuations ($\omega \ll \omega_{ci}$) a radial velocity fluctuation δv_r, due to the existence of the cross-field drift $\vec{E}_P \times \vec{B}_T$, can be written:

$$\delta \vec{v}_r = (\delta \vec{E}_P \times \vec{B}_T)/(B_T)^2.$$

To express a time average radial particle flux $\langle \Gamma \rangle = \langle n.v_r \rangle = (\langle n.E_P \rangle)/B_T$, it is necessary to measure a correlation between the radial velocity fluctuations and plasma density fluctuations:

$$\langle \Gamma \rangle = /1/B_T/.\,\langle (\langle n \rangle + \delta n).(\langle E_P \rangle + \delta E_P) \rangle =$$

$$= /1/B_T/.\,\langle n \rangle.\langle E_P \rangle + /1/B_T/.\,\langle \delta n.\delta E_P \rangle = \overline{\Gamma} + \Gamma_f .$$

The fluctuation induced flux Γ_f can be rewritten, using a cross-correlation coefficient c_{nE}, as

$$\Gamma_f = /1/B_T/.\,c_{nE}.\tilde{n}.\tilde{E}_P,$$

where symbol " $\sim$ " denotes the RMS values of quantities:

$$\tilde{n}_e = (2/A_P.c_S.E).\sqrt{\langle (\delta I_S)^2 \rangle}, \quad \tilde{E}_P = (1/d).\sqrt{\langle (\delta/\Delta U_f/)^2 \rangle} .$$

The polarity of c_{nE} determines the direction of the turbulent flux. Many tokamak experiments /17-23/ have shown that the turbulent flux at the plasma edge has mostly outwards direction and that c_{nE}=0.2-0.6, which indicates nearly complete de-correlation between density and electric field fluctuations. Nevertheless, even this value of c_{nE} is suf-

ficient to make the fluctuation-induced transport resposible for the anomalous particle losses in the tokamaks /17-23/, including CASTOR /34/.

It should be noted that besides the fluctuating poloidal field E_p a local quasistationary poloidal field E_p exists in tokamaks under some conditions. Such field, observed e.g. in JET during the ICRH /40/, in small tokamak TF-1 /41/ and recently in CASTOR /42/ as well, produces quasistationary cross-field drift $\overline{\Gamma} = \langle n_e \rangle . \langle E_p \rangle / B_T$, which can form localized regions of enhanced DC-convection.

In our experiment are the fluctuating signals processed by the three channel correlator /39/. All three channels of the correlator were absolutely calibrated and their frequency characteristics were determined. Two channel operate in the autocorrelation mode and serve for monitoring of RMS-values of density and poloidal electric field fluctuations $\tilde{n}_e$ and $\tilde{E}_p$, the third channel operates in cross-correlation mode and monitors directly the fluctuation-induced particle flux Γ_f.

The fluctuations in the central region of tokamak CASTOR were investigated using a microwave scattering technique on the wavelength λ=2.6mm/43/. The geometry of this experiment see Fig. 13. The receiving antenna system consists of 5 conical horns and two plane mirrors, enabling to detect the scattered radiation under angles ϑ_s=0,15,30,60 and 90°. These angles correspond to scattering on the fluctuations with discrete wave number $k_\perp$ in the plane perpendicular to the toroidal magnetic field $k_\perp$=6,12,24 and 34cm^{-1}. The frequency spectrum of the scattered radiation was analyzed using a homodine interferometric scheme. The scheme was absolutely calibrated. From the geometry of experiment and the absolute value of scattered wave power the spectral power density of fluctuations $S(k,\omega)$ was enumerated and by integration of this quantity over frequency and wave vector

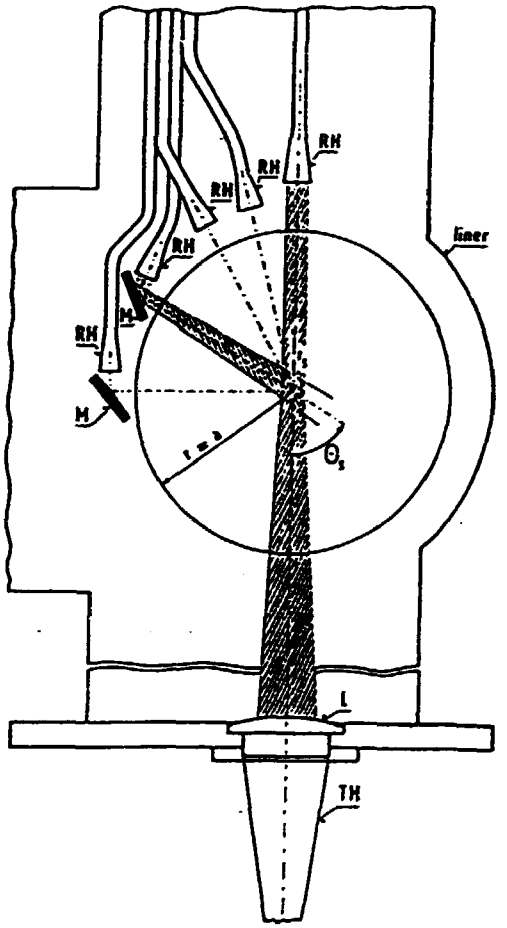

Fig. 13. Geometry of the probing and scattered beams in the small cross-section of tokamak CASTOR.

space the absolute level of density fluctuations was obtain:

$$\langle(\delta n)^2\rangle = [n/(2\pi)^4].\iint_{k\omega} S(k,\omega).d^3k.d\omega \ .$$

The movable construction of the receiving system makes us possible to measure radial profile of $\langle(\delta n)^2\rangle$.

Experimental results

Electrostatic fluctuations were studied on CASTOR in the pure inductive OH and in the combined inductive OH/LHCD regimes as well. The main experimental results can be summarized as follows:

I. OH-regime

The measurements of the edge cross-field induced par-

ticle flux in the OH tokamak regime have shown that this flux can explain the particle flux detemined from the global particle balance. A noticeable quasistationary part of this flux is observed in some cases. However, this edge cross--field induced transport exhibits a high degree of poloidal asymmetry. Therefore, the interpretation of experimental results obtained at some single specific point in the plasma should be extrapolated for whole torus with a care.

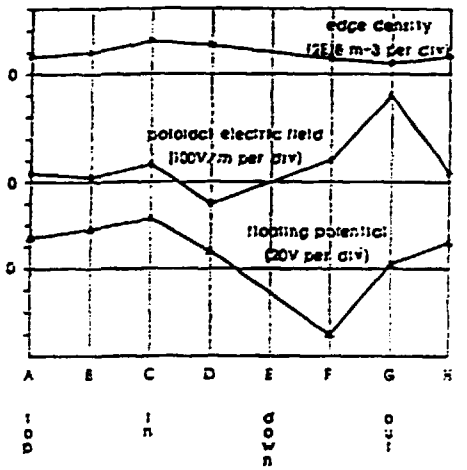

Fig. 14. Poloidal dependence of edge parameters for determination of the quasistationary flux.

The asymmetry is demonstrated in Fig. 14, which presents a poloidal variation of the edge density, quasistationary poloidal electric field E_p and floating potential V_t. It may be seen that while dependence of the edge density is approximately uniform, the E_p and V_f exhibit a very expressed maximum and they even change the direction (the $E_p < 0$) corresponds to the inward direction of the quasistationary flux $\tilde{\Gamma}$). Note that a similar asymmetry is observed for the turbulent flux component Γ_f as well /8/. A poloidally averaged value of E_p = 500V/m seems to give an outward flux of the order of $1 \times 10^{20} m^2/s$, which is comparable with the measured turbulent flux and with the particle flux determined from the global particle balance.

Some characteristic features of the electrostatic turbulence are documented in Figs. 15, 16, 17.

(1) Fig. 15 shows the radial profile of density fluctuation level measured in the outer plasma region by Langmuir probe and in the central region by microwave scattering ($k > 6cm^{-1}$) /43/.

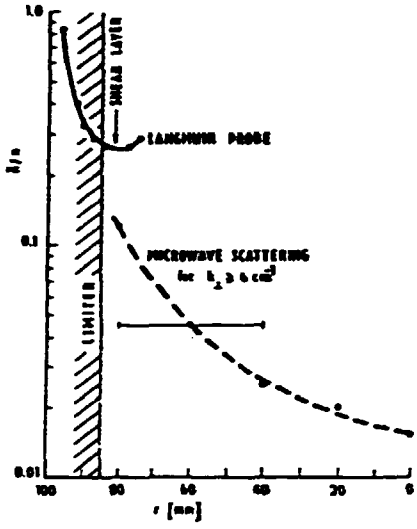

Fig. 15. Experimental observed radial profile of density fluctuation level measured by probes and by microwave scattering.

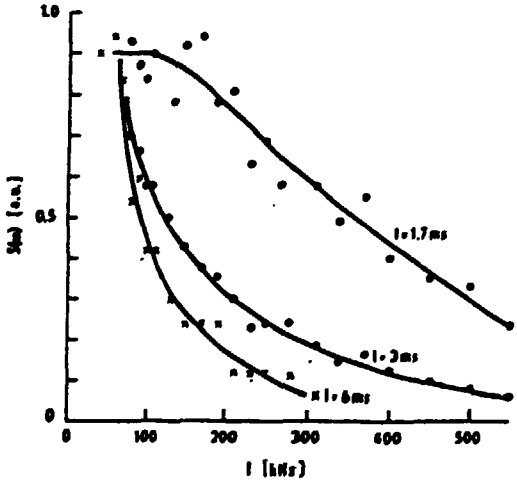

Fig. 16. Frequency spectrum of edge density fluctuation in OH regime for three time moments t=1.7, 3 and 6ms.

(2) Fig. 16 gives a time evolution of frequency spectrum of the edge density fluctuations in discharge with decreasing line average density (see n(t) e.g. in Fig. 4).

The absolute values of $\tilde{n}/n$ at the plasma edge and in

the central part of the plasma column shown in Fig. 15 and the observed narrowing of the density fluctuation spectra with decreasing density correspond well with assumption that the density gradient relaxation is dominant in the most part of the plasma /38/.

(3) Fig. 17 shows the radial profile of the floating potential V_f (a) and the profile of the poloidal electric field fluctuations (b) in the same shot series. From the figure follows that besides the poloidal component E_p of electric field the radial component E_r exists in the tokamak plasma as well /38, 42/. Due to this field the cross-field flux has an additional (poloidal) component and the pattern of plasma flow at the tokamak boundary becomes more complicated form. It may be seen from the Fig. 17 that E_r component changes even its polarity somewhere in the vicinity of the separatrix ("shear" layer). The change of polarity of the radial electric field in the near separatrix region was also deduced from the change of direction of the poloidal rotation of electrostatic fluctuations. Comparison of Figs.17a and 17b suggests also a link between the radial electric field and the level of E_p-fluctuations. The local minimum on radial profile of the E_p-fluctuations in

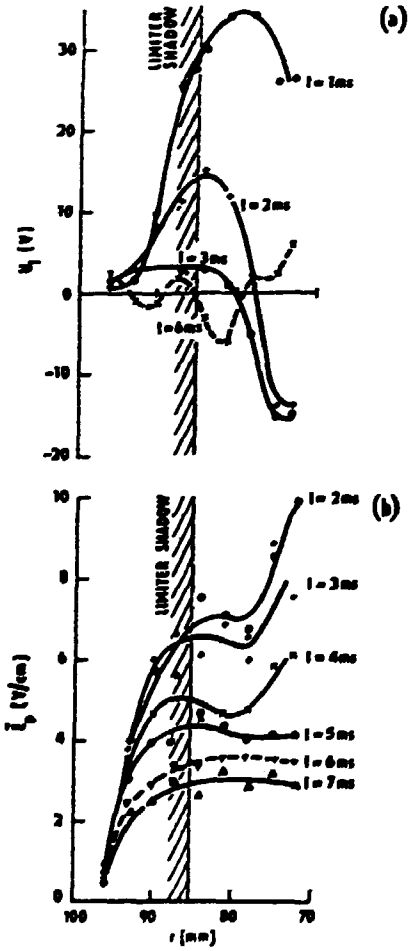

Fig. 17. Radial dependence of the floating potential V_f and its fluctuation δV_f.

Fig. 17b [illegible] minimum of density fluctuations in Fig. 15 [illegible] zero radial electric field. It indicates that the edge electrostatic fluctuations at the plasma edge [illegible] driven by the radial electric field, which provided an additional free energy source through relaxation of the density gradient /36/.

Radial electric field E_r was measured e.g. in /41,44/. It is supposed in the last time /45,46/ that just a change of this radial electric field value play an important vole in the L-H transition in tokamaks.

B) Combined OH LH current drive regime:

The specific effect observed during the injection of LH wave in the CASTOR tokamak is a considerable suppression of these fluctuations, see Fig. 18a. Fig. 19 presents the time evolutions of main plasma parameters together with the

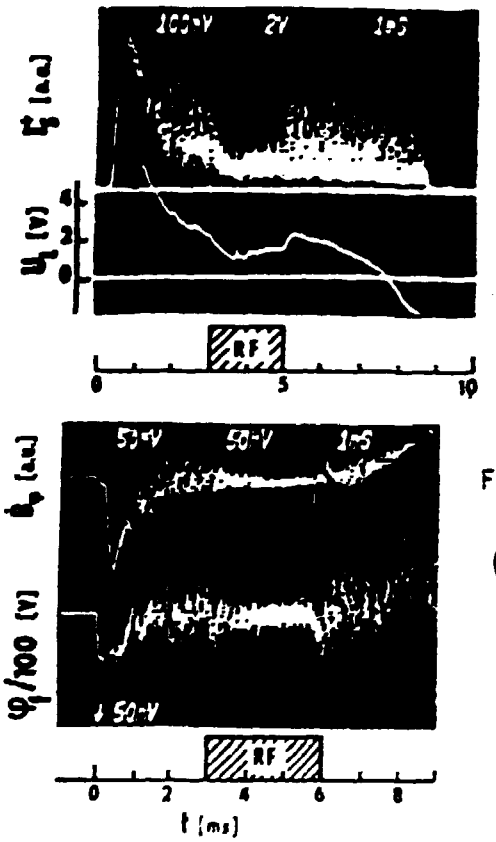

Fig. 18. a) Suppression of ion saturated current fluctuations and b) suppression of magnetic fluctuations at the RF pulse application.

turbulent characteristics n(a), $E_p(a)$ and $\Gamma(a)$ measured by triple probe at the separatrix. The dependences are given for OH (dotted lines) and OH/LHCD (full lines) regimes and for two characteristic densities. At the lower density

the RF current drive efficiency is high (Fig. 19a), at the higher density is practically zero (Fig. 19b). The OH decay of the line average density is stopped (or even changed by an increase of n_e) at the moment of the RF-power application in the both cases. It manifests an improvement of the global particle confinement. It should be emphasized that both these effects are still well pronounced near the density limit of LHCD. It should be also noted that besides of the suppression of turbulent levels, a decrease of cross-correlation coefficient c_{nE} (see its definition in the previous paragraph) is observed. It indicates some decorrelation between the n- and E- fluctuations during the suppression.

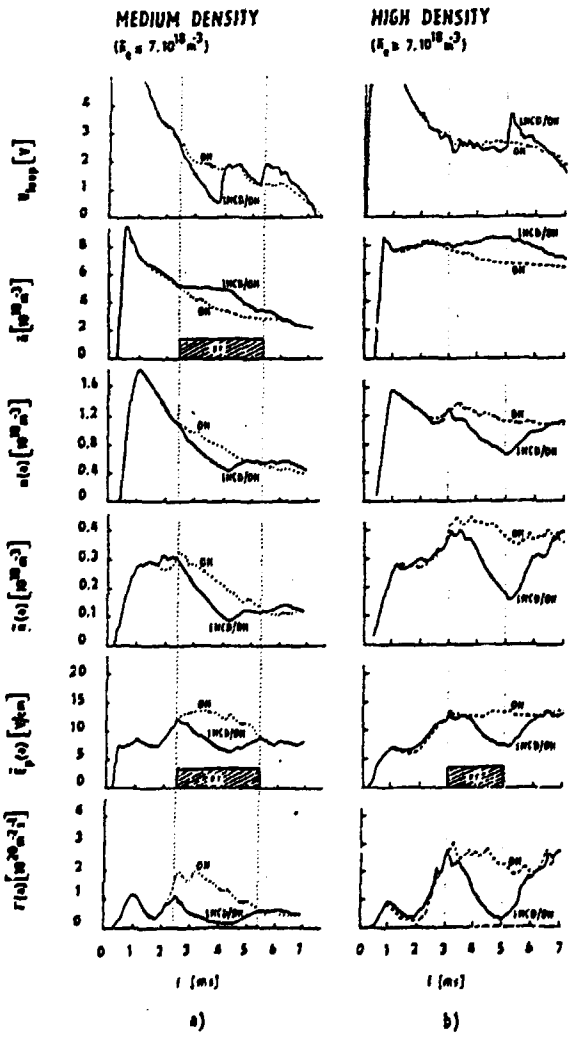

Fig. 19. Comparison of the plasma turbulent characteristics in OH and in combined OH/ /LHCD regimes for medium (a) and high (b) densities.

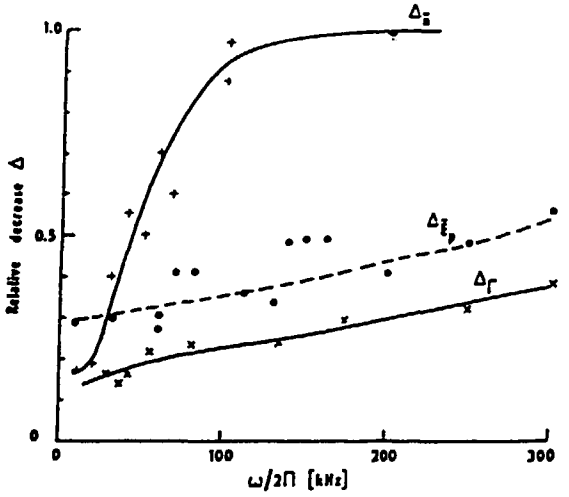

Fig. 20. Frequency dependence of relative decrease of electrostatic fluctuations and fluctuation-induced particle transport during the RF application.

Fig. 20 shows the frequency dependences of relative decrease of density fluctuations $\Delta_n = \tilde{n}^{RF}/\tilde{n}^{OH}$, electric field fluctuations $\Delta_E = \tilde{E}_p^{RF}/\tilde{E}_p^{OH}$ and turbulent flux $\Delta_\Gamma = \Gamma^{RF}/\Gamma^{OH}$ after the RF application. While the E_p-fluctuations and radial turbulent flux are suppressed in the broad frequency range by RF, only low frequency part of density fluctuations is affected ($f \lesssim 100$kHz). It also manifests that the above mentioned decorrelation between the n - and E_p-fluctuations takes place namely at higher frequences.

The improvement of the global particle/energy confinement together with the simultaneous decrease of edge electrostatic turbulence has been recently observed for $P_{RF} \lesssim P_{OH}$ on the ASDEX tokamak as well (to be published/.

3.2 Measurement of Magnetic Fluctuations and Turbulence

The effect of LHCD on MHD activity has been observed on a number of tokamaks. On ASDEX /47/, sawtooth oscillations was suppressed by LHCD simultaneously with observed broadening of current density profile and disappearance of q=1 surface. On PLT /48/ m=1 mode was suppressed despite of $q(0) < 1$. On Petula /49/, the growth of m=2 mode was stopped and maintained at low saturated level. This was also expla-

ined by a broadening of current profile, especially by decreasing of its gradient at q=2 surface. The suppression of magnetic turbulence by LHCD was reported also for the DITE tokamak /50/. In all above experiments, LHCD caused suppression of coherent MHD activity what is in agreement with theory as a result of change in current density profile /51/.

The similar effect of LHCD on magnetic turbulence was observed on the CASTOR tokamak as well /37/. For the experiments 3-waveguide multijunction grill with broad power spectrum (N_z=1-4) and rather low directivity (70%) was used. The MHD activity on this tokamak is monitored by set of 16 Mirnov coils uniformly distributed inside the liner, at the radius b=96mm, see Fig. 11. The signals from the coils are digitalized by A/D converters in the frequency band 0.1-300 kHz. An illustrative picture of poloidal magnetic field fluctuation is given in Fig. 21. It may be seen from the figure 21 that a structure rotating in the electron diamagnetic drift direction with poloidal angular velocity 1.6×10^5 r/s is well expressed.

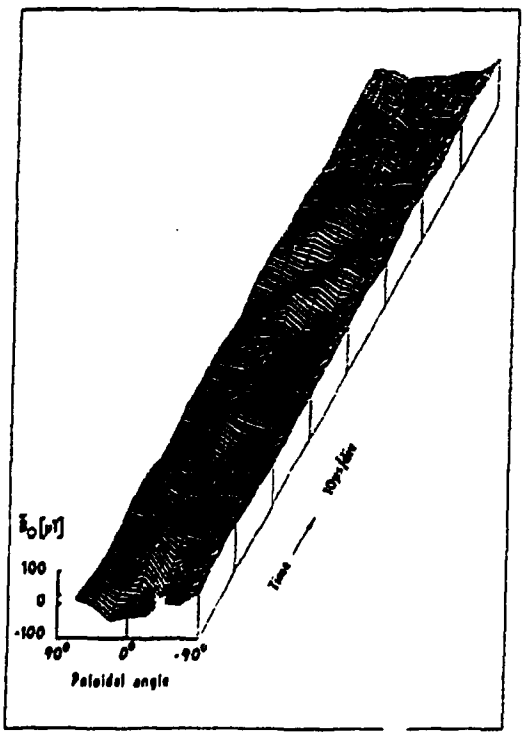

Fig. 21. A pattern of poloidal magnetic field fluctuations.

The typical effect of LHCD on magnetic turbulence is shown in Fig. 22. The relative drop of U_L indicates that at

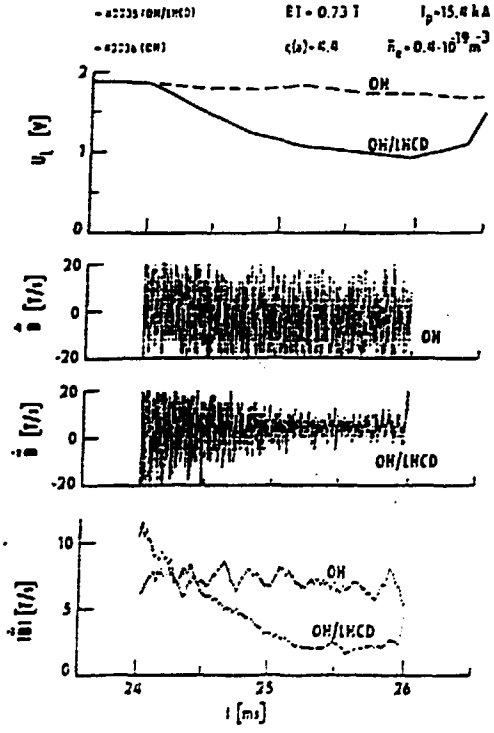

Fig. 22. Effect of LHCD on MHD activity detected by probe 14.

t=26ms half of the plasma current I_p is driven by waves. At the same time the level of MHD activity is suppressed by a factor of 2-3. Fig. 23 shows the dependence of fluctuation

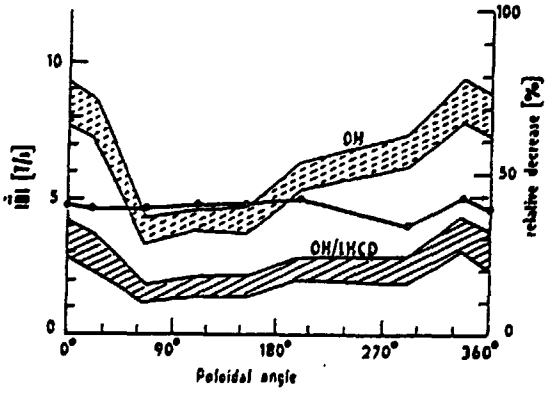

Fig. 23. Dependence of level of magnetic fluctuations on poloidal angle. The results are taken from shot in Fig. 22 by averaging fluctuation level from 25 to 26ms for probes 2,4,6,8,10,14 and 16 (angles 0 and 90^0 corresponds to probes 1 and 5 respectively).

level on poloidal angle. Despite of some modulation, the relative decrease is poloidally independent. This fact exclude the possibility that the change in fluctuation is caused only by a movement of particular magnetic surface relate to the probe as a result of increase of plasma energy during LHCD. The fast Fourier transform spectra of probes signal are shown in Fig. 24. It is seen that the effect of

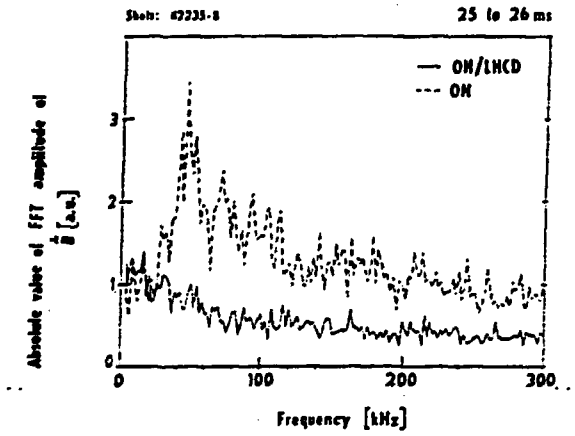

Fig. 24. Fast Fourier transform of the probe signals.

suppression takes place in a broad frequency range. Therefore, in our case, LHCD has influence on the turbulent state of plasma. It was shown in /37/ that at some iostants modes m=2 and 3 can be recognized. However, fluctuating part of magnetic signal has low coherence for both OH and OH/ /LHCD cases, see Fig. 25, and the modes live much more shorter than their revolution period and so MHD mode structure

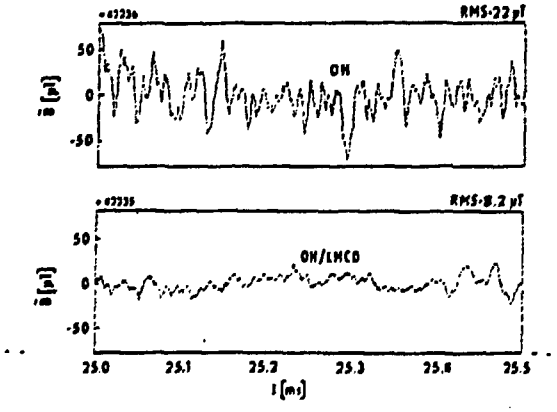

Fig. 25. Fluctuating part poloidal magnetic field calculated from probe signals in Fig. 22. The RMS values represent 6×10^{-4} resp. 2.5×10^{-4} of the total poloidal magnetic field.

exhibits a complicated behaviour.

The results concerning the MHD fluctuations can be shortly summarized as follows:

(1) a structure of MHD modes m=2 (and maybe m=3) with practically sinusoidal character in poloidal direction, rotating in the diamagnetic drift direction, is recognized in OH regime;

(2) this structure losts fully this feature in the combined OH/LHCD regimes;

(3) in the case of RF driving of about 50% of the total current the level of magnetic turbulence is suppressed by a factor 2-3;

(4) this suppression is effective in a broad band frequency region.

4. CONCLUSION

It is generally recognized that the processes in the plasma periphery play an important role in the global energy balance in tokamaks. An attempt to illustrate a complexity of these processes using some results of experimental studies on the small Prague tokamak CASTOR, was made in this paper. A special attention was paid to the study of peripheral electrostatical and poloidal magnetic field fluctuations and their modification by lower hybrid wave using a several types of multijunction grills as launching antennae. The main effect observed at the accessible RF power $P_{RF} \lesssim P_{OH}$ was the substantial suppression of these fluctuations in the tokamak regimes with combined OH/LHCD operation. Moreover, an experimentally observed occurance of radial electric field in the peripheral region and its possible role in energy balance was mentioned.

REFERENCES

/1/ Badalec J. et al., Res. rep. IPPCZ-253, p. 116, 1985
/2/ Gormezano C. et al., Nucl. Fus. 25 (1985), 419
/3/ CASTOR tokamak Group, Res. Rep. IPPCZ-256, Nov. 1985
/4/ Preinhaelter J., Res. Rep. IPPCZ-280, April 1988
Res. Rep. IPPCZ-283, June 1988
/5/ Petržílka V. et al., Czech. J. Phys. B33 (1983), 1002
/6/ Stoeckel J., Žáček F., Czech. J. Phys. B37 (1987), 201
/7/ Fedorenko S. I. et al., Res. Rep. IPPCZ-285, Nov. 1988
/8/ Weixelbaum L. et al., 9th Int. Conf. on Plasma-Surface Interaction, Bournemouth 1990, England
/9/ Badalec J., Nanobashvili S. et al., Fizika Plazmy 14 (1988), 395
/10/ Budnikov V. N. et al., Fizika Plazmy 11 (1985), 53
/11/ Valovič M., Czech. J. Phys. B38 (1988), 65
/12/ Parail V. V. et al., Fizika Plazmy 15 (1989), 1390
/13/ Soeldner F. X. et al., Res. Rep. IPP III/111, Garching 1986
/14/ Nanobashvili S. et al., Czech. J. Phys. B37 (1987), 194
/15/ Kopecký V. et al., Plasma Physics 17 (1975), 1147
/16/ Liewer P. C., Nucl. Fusion 25 (1985), 543
/17/ Rowan W. et al., Nucl. Fus. 27 (1987), 1105
/18/ Ritz C. P. et al., Nucl. Fus. 27 (1987), 1125
/19/ Zweben S. J., Gold R. W., Nucl. Fus. 25 (1985), 171
/20/ Howling A. et al., 12th Europ. Conf. on Contr. Fus. and Plasma Phys., Budapest 1985, Proc. I, 311
/21/ Budaev V. P., Ivanov R. S., 12th Europ. Conf. on Contr. Fus. and Plasma Phys., Budapest 1985, Proc. I, 303
/22/ Levinson S. J. et al., Nucl. Fus. 24 (1984), 527
/23/ Zweben S. J., Taylor R. J., Nucl. Fus. 23 (1983), 513
/24/ Macalarne M., Duperrex P. A., JET-P (87) 26, May 1987
/25/ Dodel G. et al., IPP III/120, p.59,Garching, June 1987
/26/ Alikaev V. V. et al., Fizika Plazmy 11 (1985), 53
/27/ Luckardt S. C. et al., Phys. Fluids 29 (1986), 1985
/28/ Mayberry M. J. et al., Phys. Fluids 30 (1987), 2288

/29/ Alikaev V.V. et al., 11th Int. Conf. on Plasma Phys. and Contr.Nucl.Fus. Res., Kyoto 1986, IAEA-CN-47/F-II-4

/30/ Takase Y. et al., Nucl. Fus. 27 (1987), 53

/31/ Stevens J. E. et al., 12th Europ. Conf. on Contr. Fus. and Pl. Phys., Budapest 1985, Proc. II, 192

/32/ Parlange F. et. al., 12th Europ. Conf. on Contr. Fus. and Pl. Phys., Budapest 1985, Proc. II, 172

/33/ Soedner F. et al., 12th Europ. Conf. on Contr. Fus. and Pl. Phys., Budapest 1985, Proc. II. 244

/34/ Stoeckel J. et al., IPPCZ-279, Prague 1988

/35/ Stoeckel J. et al., 12th Int. Conf. on Pl.Phys. and Contr. Nucl. Fus., Nice 1988, Nucl. Fus. Supplement 1989, Vol. 1, 359

/36/ Stoeckel J. et al., IPPCZ-293/II, 157, Liblice 1989

/37/ Valovič M., IPPCZ-300, Prague 1990

/38/ Vlad M. et al., IPPCZ-293/II, 174, Liblice 1989

/39/ Kryška L., Stoeckel J., Res. Rep. 22/88, IPP Prague 1988

/40/ Clement S. et al., 16th Europ. Conf. on Contr. Fus. and Pl. Res., Venice 1989

/41/ Budaev V.P. et al., 9th Int. Conf. on Plasma-surface Interaction, Bournemouth 1990, England

/42/ Stoeckel J. et al., 13th Int. Conf. on Pl. Phys. and Contr. Fus. Res., IAEA-CN-53/A-7-2, Washington 1990

/43/ Valovič M. et al., Fizika plazmy 15 (1989), 515

/44/ Groebner R. J. et al., Phys. Rev. Lett. 64 (1990),3015

/45/ Biglari H., Diamond P. H., Phys. Fluids B2 (1990), 1

/46/ Shaing K. C., Crume E. C., Phys. Rev. Lett. 63 (1989), 2369

/47/ Soeldner F. X. et al., Phys. Rev. Lett. 57 (1986),1137

/48/ Chu T. K. et al., Nucl. Fus. 26 (1986), 667

/49/ Van Houtte D. et al., Nucl. Fus. 24 (1984), 1485

/50/ Robinson D. C., Proc. of the Cadarache Workshop on Electrostatic Turbulence, EUR-CEA-FC-1381, p. 1, 1989

/51/ Yoshioka Y. et al., Nucl. Fus. 24 (1984), 565